frontiers | Frontiers in Earth Science

TYPE Original Research
PUBLISHED 07 January 2025
DOI 10.3389/feart.2024.1384098

OPEN ACCESS

EDITED BY
Claudia Belviso,
National Research Council (CNR), Italy

REVIEWED BY
Steven J. Schatzel,
Centers for Disease Control and Prevention (CDC), United States
Caifang Wu,
China University of Mining and Technology, China

*CORRESPONDENCE
Yuqiang Jiang,
xnsyjyq3055@126.com

RECEIVED 08 February 2024
ACCEPTED 16 December 2024
PUBLISHED 07 January 2025

CITATION
Zhuang H, Jiang Y, Li X, Jiang C, Li S and Wang Z (2025) Geochemical characteristics and organic matter accumulation mechanism of the Permian Shanxi Formation transitional shale, eastern Ordos Basin: implications for paleo-weathering, provenance and tectonic setting.
Front. Earth Sci. 12:1384098.
doi: 10.3389/feart.2024.1384098

Geochemical characteristics and organic matter accumulation mechanism of the Permian Shanxi Formation transitional shale, eastern Ordos Basin: implications for paleo-weathering, provenance and tectonic setting

Hongzhan Zhuang[1,2], Yuqiang Jiang[1,2]*, Xingtao Li[3], Chan Jiang[4], Shuxin Li[3] and Zhanlei Wang[1,2]

[1]School of Geoscience and Technology, Southwest Petroleum University, Chengdu, China, [2]The Unconventional Reservoir Evaluation Department, PetroChina Key Laboratory of Unconventional Oil and Gas Resources, Chengdu, China, [3]PetroChina Coalbed Methane Company, Beijing, China, [4]Exploration Division, PetroChina Southwest Oil and Gas Field Company, Chengdu, China

The transitional shale of the Permian Shanxi Formation is an important source rock for shale gas, tight sandstone gas, and coalbed methane in the Ordos Basin. This study takes third Sub-Member of Shanxi Formation as an example, and uses continuously collected shale core samples and matching geochemical data to restore the paleo-environmental conditions of its depositional period, clarify the formation mechanism of organic rich shale in different sedimentary environments under transitional facies background. According to different types of cross-plot patterns, paleo-weathering, provenance sources, and tectonic backgrounds were determined in this study. The results indicate that Shanxi organic-rich shale can be divided into two categories: estuarine shale in Unit 1 and lagoon shale in Units 2–4. The average TOC value of estuarine shale is significantly higher than that of lagoon shale, reaching 5.55%. Estuarine shale is mainly deposited in an suboxic-anoxic bottom water environments, with high surface seawater productivity, which is conducive to the formation and preservation of a large amount of organic matter. Lagoon shale is mainly composed of Type II_2 and III kerogen, with a weakly oxic bottom water environment and low water surface paleo-productivity. The organic matter mainly comes from terrigenous plant debris, and its high sedimentation rate can effectively accumulate and preserve it. The chemical weathering indicators of Shanxi transitional shale are controlled by sedimentary recycling, hydrodynamic sorting, and diagenetic alteration, and the influence of changes in the source area is relatively small. The Shanxi transitional shale is mainly deposited on the active continental margin under

collision background, and its source is mainly granodiorite from the Qinling orogenic belt.

KEYWORDS

transitional shale, organic matter accumulation, paleo-weathering, provenance, tectonic setting, Ordos Basin

Introduction

Shale gas is an important unconventional energy source, and its exploration and utilization began in the United States (Zou et al., 2020; 2022). Over the past twodecades, it has become a major focus for exploration and production companies in many countries, including China (Zou et al., 2020). The Shanxi Formation of the Permian in the Ordos Basin is rich in tight sandstone gas, shale gas, and coalbed methane (Wu Z. Y. et al., 2021; Zhang et al., 2022). Previous work has mainly focused on the research of coalbed methane and tight sandstone gas, although it is known that the black shale of the Shanxi Formation containing coal is composed of organic-rich rock intervals (Kuang et al., 2020; Xu et al., 2023). The organic rich sediments of the Permian Shanxi Formation in Ordos mainly exist in the second section, including black mudstone, shale, and thin coal seams of lagoon, estuarine, and pre-delta facies (Gu et al., 2022). Zhang et al. (2021) think that the shale intervals of the Lower Shanxi Formation were deposited in a lagoon environment with high detrital influx input and oxic sedimentary environment. Zhao et al. (2021) consider that the organic matter was mainly derived from terrestrial plants and its accumulation was predominately controlled by abundant terrigenous plants input, redox conditions and paleoclimate. However, previous studies have mainly describe the geochemical characteristics and paleoenvironment evolution of black shale in a single sedimentary facies of Shanxi Formation transitional shale (Gu et al., 2022; Jiang et al., 2023), and have not yet systematically evaluated the formation mechanism in different sedimentary facies, including the evaluation of the source of fine-grained sediments, tectonic setting, and paleo-weathering conditions (He et al., 2022; Jiao et al., 2023; Wang et al., 2023).

Well A is a key shale gas exploration well in the eastern part of the Ordos Basin, and it is currently the most complete drilling core data of the Permian Shanxi Formation in the Ordos Basin (Kuang et al., 2020; Jiao et al., 2023). By utilizing the entire core of this well, this study will combine the changes in multiple geochemical proxies related to paleo-redox conditions, paleo-productivity, paleo-climatic conditions, and debris sediment flux with the stratigraphic framework to determine the main mechanisms of organic matter accumulation in different shale units of the Shanxi Formation. In addition, we also utilized the content of major and trace elements to study changes in sediment sources, tectonic environments, paleoweathering, and various influential non paleoclimatic factors. The results of this study provide a basis for understanding the formation mechanism and characteristics of shale reservoirs in the Shanxi Formation of the Ordos Basin.

Geological setting

The Ordos Basin is located in the western part of the North China Craton, between the Qinling Mountains and the Yinshan Mountains in the north and south (Liu et al., 2023). In the Late Paleozoic, the Ordos Basin experienced a major cycle of transgression and regression. In the early stage, it was the stage of land surface sea filling. In the late Early Permian, seawater rapidly receded from the Ordos region. In the middle to late Permian, it was the stage of evolution of nearshore and continental lacustrine-basins. Seawater entered from northeast to southwest, developing a thick set of coal-bearing deposits between sea and land, forming the most important coal and gas bearing strata in the Ordos Basin, achieving the transition from marine sedimentation to terrestrial sedimentation. Controlled by the cycle of transgression and regression, transitional shale was formed within the Permian Taiyuan Formation and Shanxi Formation. The study area is located in the eastern part of the Ordos Basin (Figure 1A). Previous studies have shown that the transitional organic-rich shale interval of the Shanxi Formation is located in the third Sub-Member of the lower part of the Shanxi Formation (Jiang et al., 2023; Jiao et al., 2023). For the convenience of oil and gas exploration and development, the third Sub-Member can be further divided into four units (Gu et al., 2022). The organic-rich shale of Unit 1 was formed in estuarine environments, while the organic-rich shale of Unit 3 was formed in lagoon environments (Figure 1B). There are significant differences in mineral composition, gas content, and pore structure between these transitional shales (Jiang et al., 2023).

Methods

Sample preparation

This study carried out continuous coring in Shanxi black shale with 37 samples. From Unit 1 to Unit 4, the sample quantity respectively are 11, 8, 8 and 10. 125 thin sections of core samples were made and the core observation results were further verified by Leica DM4 M optical microscope. Observation and description of typical sections were made in the study area, with emphasis on sedimentary texture or structure.

Organic matter contents analysis

TOC were measured by Leco carbon/sulfur analyzer in PetroChina Key Laboratory of Unconventional Oil and Gas Resources, and the analytical precisions are ±0.5%. The samples were treated with 10% hydrochloric acid to remove carbonates. The acid

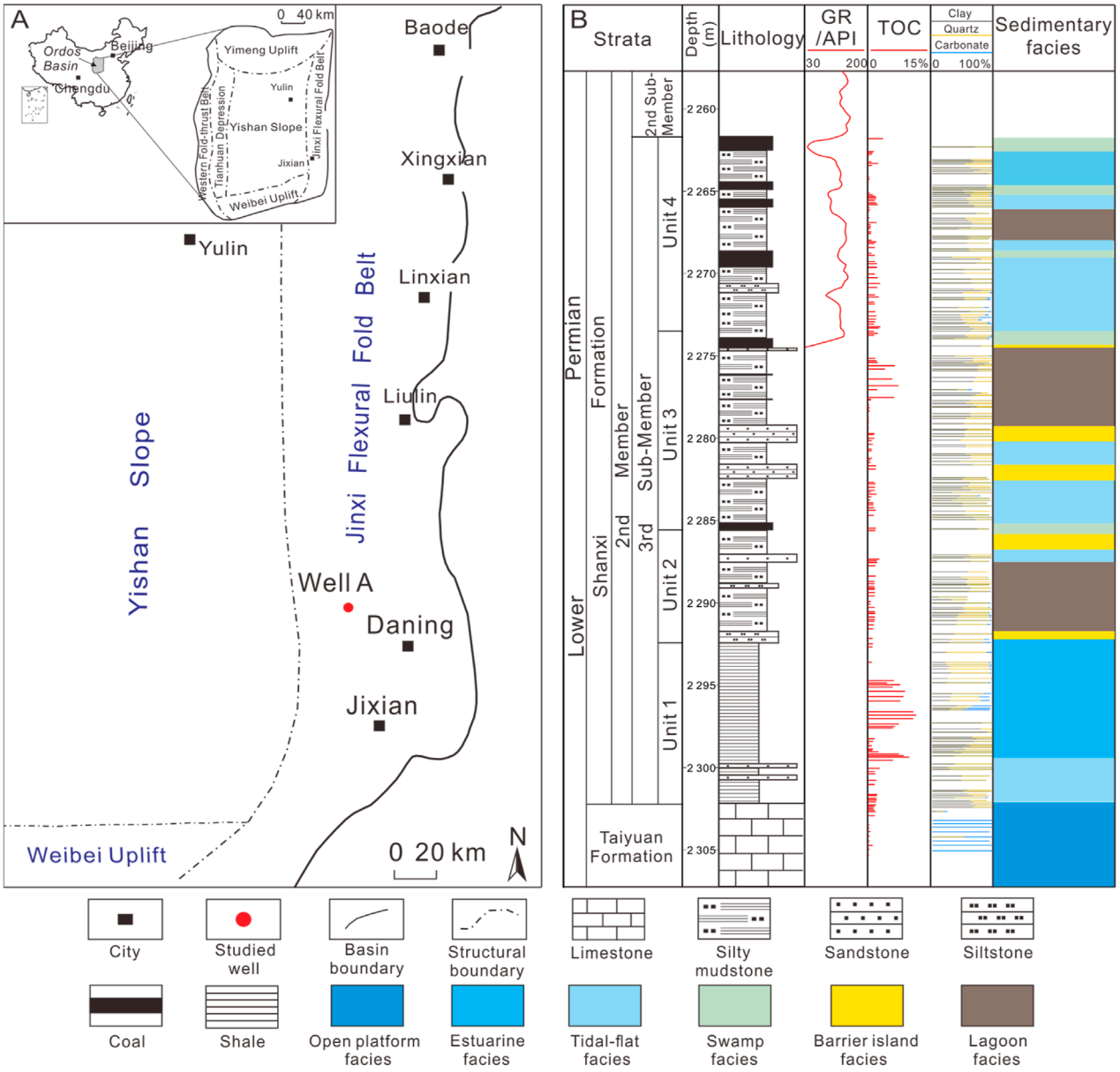

FIGURE 1
(A) Location of the Well A and **(B)** an stratigraphic histogram of Shanxi Formation shale interval in the study area.

treated sample was washed with distilled water to neutral, then the sample was dried in an oven at 60°C–80°C. Dried samples were added to the cosolvent and fully burned in the high-temperature oxygen flow, ensuring that the organic carbon can be completely converted into carbon dioxide, and the content of total organic carbon was tested by infrared detector.

Mineralogical composition analysis

Mineralogy and mineral compositions were determined and measured for 125 remaining samples corresponding to thin section identification, which do not correspond to the samples used for geochemical analyses, with a Rigaku SmartLab9 rotating anode X-ray diffractometer using 40 kV and 100 mA with a Cu Ka radiation. Stepwise scanning measurements were performed at a rate of 4°/min in the range of 3°–85°(2θ). The analytical uncertainties of XRD mineralogy analysis are estimated to be 2%. The relative mineral percentages were estimated using K-value method. K-value is the positive correlation between the content of a certain mineral and the intensity of its characteristic diffraction peak. Quartz, carbonates, and clay minerals among the major minerals are shown in Figure 1B.

Element composition analysis

The concentration of major elements was determined by X-ray fluorescence (XRF) spectroscopy. The powder samples were used to eliminate the mineral and grain size effects, and cast to a suitable fused glass beads to fit the X-ray fluorescence spectrometer.

The fluorescent X-ray intensity of the elements were measured. According to the calibration curve or equation, the interference effect between elements was corrected and the element content was obtained. The accuracy of the XRF analysis is better than 1% for all major oxides.

Trace and rare elements were measured by using inductively coupled plasma-mass spectrometry (ICP-MS). The samples were dissolved by hydrofluoric acid and nitric acid in a closed container. The hydrofluoric acid was wiped out by evaporation on the electric heating plate, and then dissolved by nitric acid. After dilution, the samples were directly measured by ICP-MS. The analytical uncertainties are estimated to be 5%. Standard rock reference material (GSD-9) were used to monitor the analytical accuracy and precision.

Results

TOC content characteristics

Based on testing data, this study sorted out the TOC changes in each unit of third Sub-Member (Figure 2A). The TOC varies widely in Unit 1, and rang from 0.26% to 10.96%, with an average of 5.55% (n = 11). The high TOC values are concentrated in 2294.5 m–2300.27 m. The TOC range in Unit 2 is small, distributed in 0.59%–2.14%, the average is only 1.41% (n = 6). In the Unit 3, the range of TOC is 0.14%–7.32%, with an average of 1.83% (n = 8). The abnormally high TOC values are concentrated in 2276.5 m–2278.12 m. In Unit 4, the range of TOC is only 0.24%–2.55%, with an average of 1.57% (n = 10).

Geochemical characteristics of elements

Major elements

The major elemental oxides in Shanxi shale are SiO_2, Al_2O_3, and Fe_2O_3, with an average of 58.4%, 18.75%, and 3.71%, respectively. The mean distribution of each unit after UCC standardization is shown in Figure 2B. Compared to PAAS, NASC, and UCC standard shale, the Ca, Mg, and Na elements in Shanxi shale exhibit significant depletion, with only Al and Ti elements showing relative enrichment in specific intervals. Ca element is enriched in Unit 1 compared to other units, which may be due to the abundance of calcareous biofossils and authigenic carbonate particles in the estuarine shale (Gu et al., 2022). The Na_2O content is significantly lower, indicating a lower content of plagioclase in the source rock, which may be related to the acidic magmatic rock source.

Trace elements

After UCC standardization, the vast majority of trace elements were not distributed near the baseline (Figure 2C), and the same element did not show consistent relative enrichment or depletion in different units (Figure 2C), such as Mo, Hf, Sc, etc. The distribution and amplitude of trace elements relative to the UCC baseline are inconsistent, which fully indicates that the sedimentary environment changes rapidly. Compared with Unit 1, the content of elements such as B, Zr, Hf, Sc, Ga, etc., in other units is significantly higher, indicating that the terrestrial input of the latter is significantly larger.

Rare elements

The total amount of rare earth elements is distributed between 30.63 and 912.86 ppm, with an average of 278.65 ppm. After standardization, the distribution of REE in each unit of chondrite is similar to that of PAAS, NASC, and UCC, all showing significant enrichment of light rare earths, flat distribution of heavy rare earths, and weak negative Eu anomalies (Figure 2D). The distribution of REE in different units is basically consistent, with poor differentiation, which may be related to the relatively stable and single source of rare earths during sedimentation. The subtle differences in the distribution of rare earth elements in different units may reflect changes in sedimentary processes such as mineral composition, hydrodynamic sorting, chemical weathering, or sediment recycling in the provenance region.

Discussion

Transition shale formation mechanism in Shanxi Formation

Paleo-productivity

P and Cu elements, as the main nutrients for life reproduction or biological activities, are commonly used to qualitatively reflect the paleo-productivity of water bodies (Tribovillard et al., 2007; Li et al., 2020). In order to eliminate the influence of terrestrial debris, P/Al and Cu/Al were used in this study to indicate the level of paleoproductivity, with high values indicating high paleoproductivity levels. In Figure 3, the evolutionary trends of P/Al and Cu/Al are consistent, indicating that paleoproductivity is higher in the upper part of Unit 1, followed by Unit 3 and Unit 2, which is consistent with the results of Figure 4A. The credibility of productivity indicators will be severely affected by the redox conditions, debris input, and diagenetic alteration effects (Pan et al., 2020). Therefore, referring to the method proposed by Schoepfer et al. (2015), Ba was used as a semi quantitative calculation of paleoproductivity levels as a biological element content (Wu J. et al., 2021). The results showed that during the sedimentation process of the Shanxi Formation shale, there was a significant change in the level of paleoproductivity, ranging from 1.6 to 3401.84 g $cm^{-2}kyr^{-1}$. Unit 1 had the highest average of 598.79 g $cm^{-2}kyr^{-1}$, while Unit 4 had the lowest average of 119.58 g $cm^{-2}kyr^{-1}$. This also confirms that Unit 1 has the highest paleoproductivity in the surface water. In addition, Unit 1 was rich in quartz mineral, which may be formed with more siliceous biological bones under high productivity (Zhao et al., 2017).

Paleoredox

Redox sensitive element enrichment factor (U_{EF} and Mo_{EF}) were widely used to determine the redox conditions of paleo-water, and the smaller these proxies reflect the higher oxidation degree (Rimmer, 2004; Algeo and Liu, 2020). The variation trend of U and Mo enrichment factors after UCC standard correction and

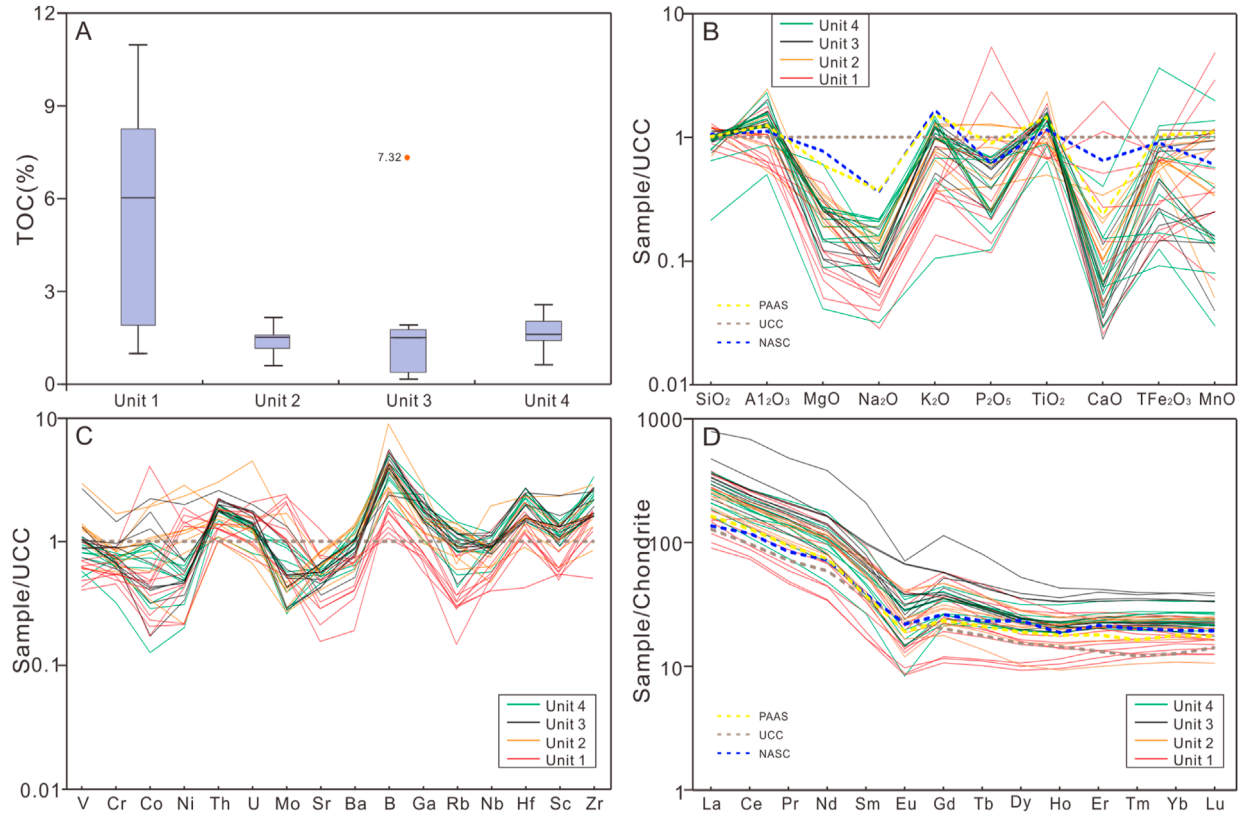

FIGURE 2
Box diagram of TOC distribution within Shanxi shale. **(A)** Concentration coefficient distribution of the major **(B)** and trace element **(C)** after UCC-normalization. Chondrite normalized REE distribution curves for REEs **(D)** UCC, PANS, NASC and Chondrite values are from Wedepohl (1995), Condie (1993) and Lodders and Fegley (1998).

calculation is basically consistent in the Shanxi Formation shale interval (Wedepohl, 1995). The average values of U and Mo are highest in Unit 1, at 1.75 and 1.94, respectively, followed by Unit 2, indicating that the reduction conditions of bottom water in Unit 1 are the best (Figure 3). Ni/Co vs. U/Th (Figure 4B) and U_{EF} vs. Mo_{EF} (Figure 4C) also indicate that Unit 1 has the strongest bottom water reducibility and is in an suboxic-anoxic environment (Jones and Manning, 1994; Tribovillard and Algeo, 2009). A high value of C_{org}/P_T can also indicate that the bottom water has strong reducibility (Wu J. et al., 2021), but it is affected by the TOC content during use (Algeo and Ingall, 2007; Xu et al., 2020). The C_{org}/P_T values of high TOC samples in Unit 1 and Unit 3 were significantly higher (Figures 3, 4D), indicating a strong P cycle under reducing conditions, which not only provides abundant nutrient supply but also facilitates burial preservation (Xu et al., 2020; Lei et al., 2023). However, under low TOC conditions, high values of C_{org}/P_T may be related to less supply of P element. In addition, the four high TOC samples in the upper part of Unit 1 have high productivity (Figure 4A) and are in an anoxic environment (Figure 4C), but their Fe/Al values are as high as 60 (Figure 4D). It is suggested that this phenomenon is related to the intermittent upwelling of seawater in estuaries during the sedimentation of Unit 1, which brings Fe element replenishment and is beneficial for improving productivity and promoting organic matter accumulation.

Detrital influx

The content of Zr, Ti, and Al elements is often used to analyze the intensity of terrestrial inputs (Li et al., 2020; Wu J. et al., 2021). The Zr/Al ratio is considered an effective indicator for quantifying the flux of non aluminosilicate source debris, with high Zr/Al ratios representing large particles and relatively high deposition rates (Böning et al., 2004; Zhang et al., 2021). The variation in Zr content reflects that the input of terrestrial debris gradually decreases within Unit 1, while it shows a continuous increasing trend in Unit 2, Unit 3, and Unit 4 (Figure 3). The Zr/Al values show a gradually decreasing trend in Unit 1 and Unit 2, while increasing gradually in Unit 3 and Unit 4. The low values of Unit 2 and Unit 3 indicate a higher proportion of clay in the terrestrial debris during their sedimentary period, which is consistent with changes in mineral composition (Figure 1B). The differentiation of rare earth elements is also commonly used to indirectly characterize the sedimentation rate (Tyson, 2001). The NASC standardized $(La/Yb)_N$ deviated from 1 in the early sedimentation of Unit 1 and Unit 3, indicating the slowest sedimentation rate during this period. Conversely, the sedimentation rate was highest in Unit 2 and Unit 4. The correlation between Zr and Zr/Al is poor within the Shanxi shale interval (Figure 4E), which indirectly reflects the variability of debris supply methods and does not have a single stable provenance.

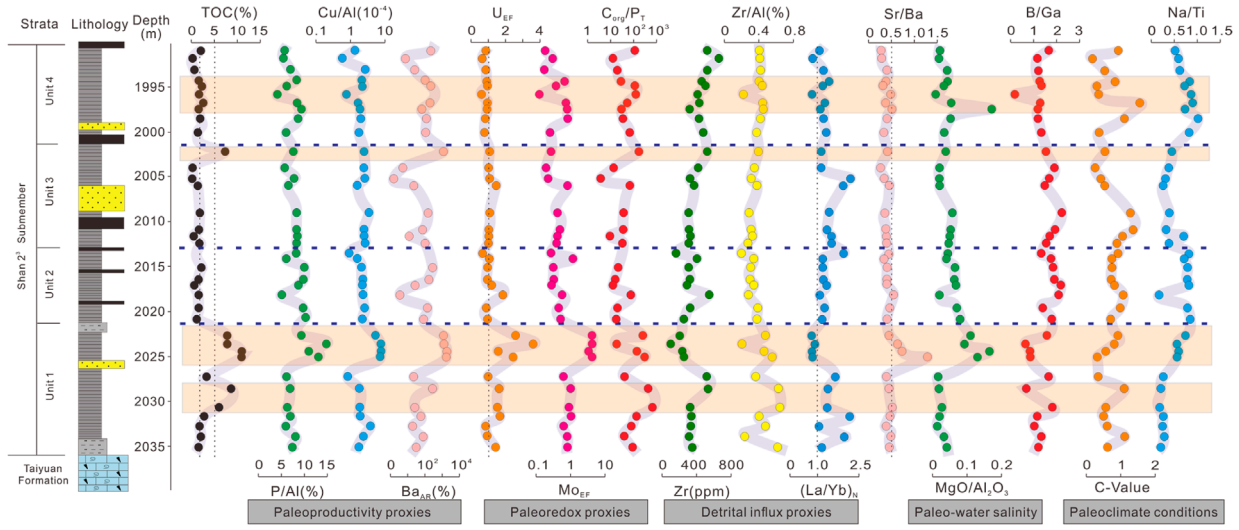

FIGURE 3
The distribution of geochemical indicators in the Shanxi shale.

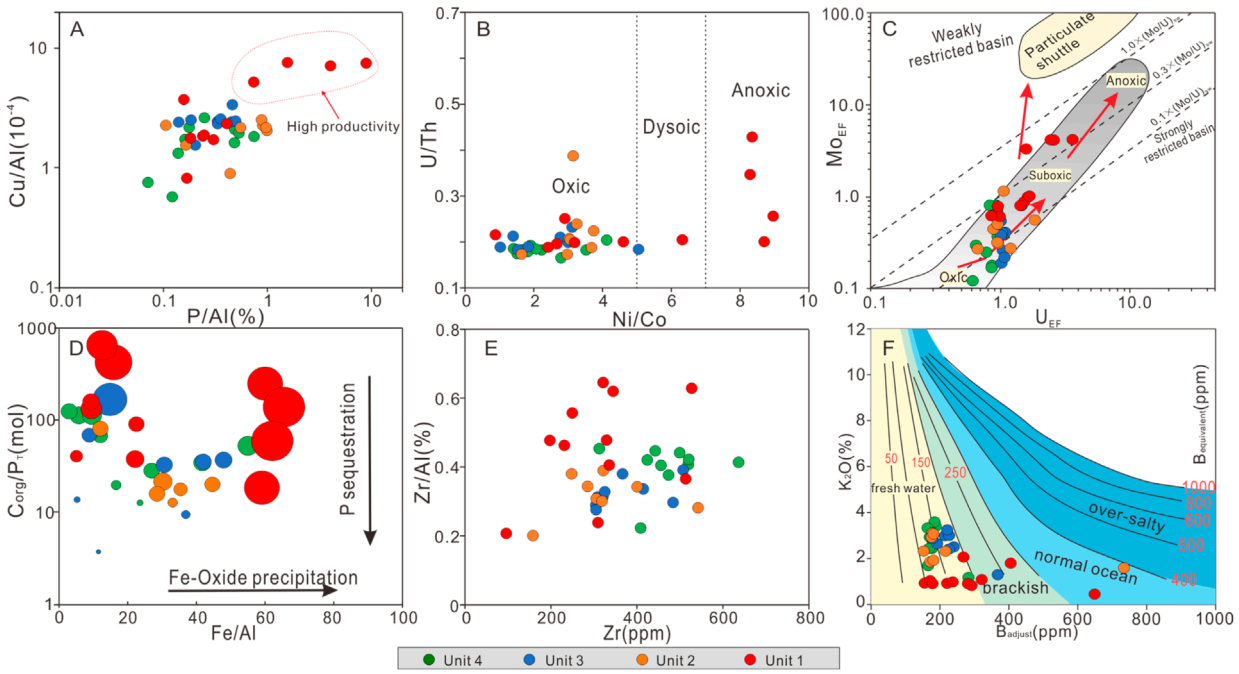

FIGURE 4
Cross-plots of **(A)** P/Ali versus Cu/Al **(B)** U/Th versus Ni/Co, **(C)** U_{EF} versus Mo_{EF}, **(D)** Fe/Al versus C_{org}/P_T, **(E)** Zr versus Zr/Al and **(F)** B_{adjust} versus K_2O in the Shanxi shale.

Paleoclimate

C-value is considered an effective indicator for evaluating paleoclimate, with higher C-values generally indicating more humid climates (Zhao et al., 2017; Li et al., 2020). The C value distribution in the Shanxi shale interval ranges from 0.19 to 1.56, with an average of 0.74, indicating an overall humid environment. From a vertical evolution perspective, the average C-value within Unit 2 is the highest at 0.84, suggesting that the climate in Unit 2 is the wettest. However, its distribution indicates that Unit 3 and Unit 4 were also in a relatively humid climate in the early stages. Alkali metal elements represented by Na are prone to dissolution and loss in humid environments, while heavy mineral elements such as Ti are less likely to migrate. The higher the ratio, the wetter the climate (Liu et al., 2022). Based on the distribution of Na/Ti, it can be inferred that the climate during the sedimentation period of Unit 2 and Unit 4 was the wettest.

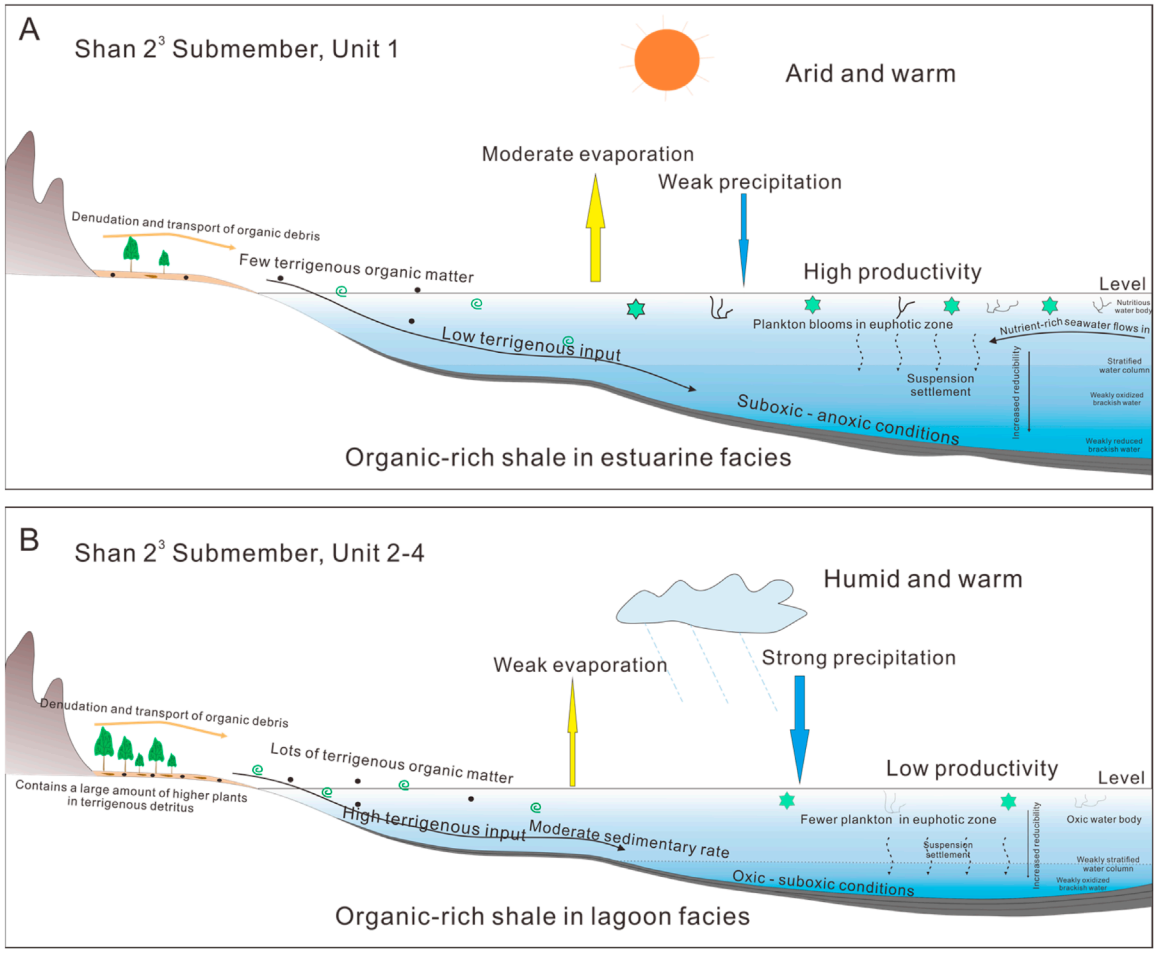

FIGURE 5
Sedimentary model of transitional organic-rich shale for estuarine facies **(A)** and lagoon facies **(B)** in Shanxi Formation.

Paleo-water salinity

Sr/Ba, MgO/Al_2O_3, and B/Ga are commonly used indicators for restoring paleosalinity in water bodies. The Sr/Ba ratio can be divided into three intervals, namely, greater than 0.5, 0.2 to 0.5, and less than 0.2, representing marine, brackish, and freshwater environments, respectively (Wei et al., 2018; Wei and Algeo, 2019; Qiu and He, 2022). There is no significant correlation between Sr and CaO in the shale section of the Shanxi Formation, so there is no need to calibrate the Sr content. The Sr/Ba ratio is distributed between 0.27 and 1.32, with a mean of 0.46, and the vertical distribution shows a slow decreasing trend. It has been proven that during the sedimentation of shale in the Shanxi Formation, the water body was in a semi saline environment, and only Unit 1 and Unit 2 in the early stage belonged to intermittent marine transgressive sedimentation, which is consistent with the estuarine environment. The variation of MgO/Al_2O_3 is consistent with the Sr/Ba ratio, but the evolution trend of B/Ga is consistent with that of C-value. It is suggested that the B content is strongly influenced by the input of terrestrial debris, and B/Ga is meaningless. The corrected B content indicates the presence of marine sedimentary traces in Unit 1 and Unit 2 (Sun et al., 2022). But most of the samples are still deposited in freshwater environments (Figure 4F), which is inconsistent with the Sr/Ba results. However, referring to the conclusion of Zhang et al. (2021), it is suggested that Unit 3 and Unit 4 were deposited in a brackish water environment.

Transition shale formation mechanism

The Shanxi organic-rich shale interval includes the estuarine shale in the upper part of Unit 1 and the lagoon shale in Units 3 and 4 (Figure 3). Regarding the genesis of high TOC intervals in shale, previous studies have commonly used "productivity models," "preservation models," and "multi factor co control" to analyze (Zou et al., 2019; Xu et al., 2020; Wu Z. Y. et al., 2021; Lei et al., 2023). Based on previous studies (Gu et al., 2022; Tan et al., 2023; Jiao et al., 2023), this study attempts to propose a sedimentary model of organic-rich shale in the Shanxi Formation based on various geochemical indicators (Figure 5).

During the Taiyuan period, the Ordos Basin developed a wide range of epeiric sea platforms with gentle slopes, which easily formed a large area of shallow water, and even slight sea level changes can alter the spatial distribution of sedimentary facies (Zhang et al., 2021; Gu et al., 2022). Unit 1 inherited the sedimentary background of the Taiyuan period, and with the rapid rise of sea level, the study area quickly turns into estuarine facies. During this period (Figure 5A), the climate is relatively dry, the impact of terrestrial debris input is limited, and the depth and salinity of the water body are conducive to

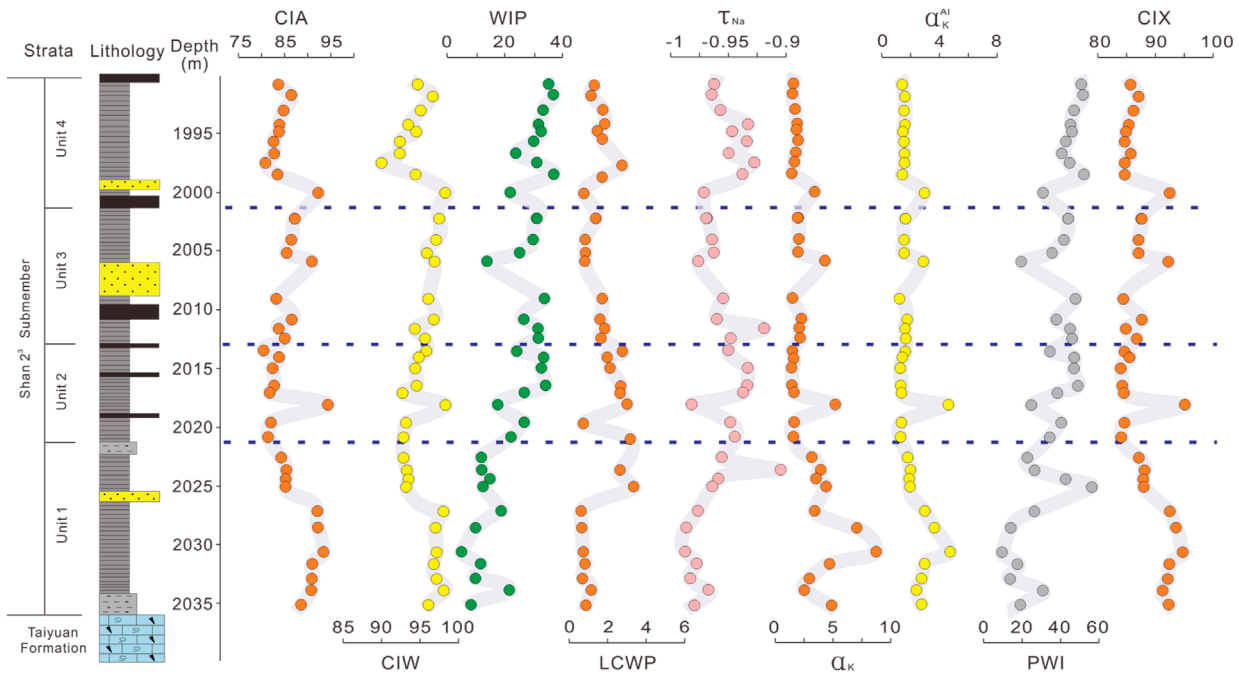

FIGURE 6
Stratigraphic lithology variations and values of representative weathering indices. CIA (Chemical index of alteration) (Nesbitt and Young, 1982), CIW(Chemical index of weathering) (Harnois, 1988), WIP (Weathering index of Parker) (Parker, 1970), LCWP (Loss chemical weathering proxy) (Yang et al., 2006), τNa(Chemical weathering depletion of Na) (Rasmussen et al., 2011), αK (Elemental weathering indices) (Gaillardet et al., 1999) and αAlK (Garzanti et al., 2013), PWI(Paleosol weathering index) (Gallagher and Sheldon, 2013), CIX (Modified chemical index of alteration) (Garzanti et al., 2014).

density stratification. The bottom water conditions are in an suboxic-anoxic conditions, and the nutrients brought by seawater circulation are conducive to the reproduction of seawater surface organisms, all of which are beneficial to the large-scale preservation of organic matter. During the sedimentation period of Unit 2–4 (Figure 5B), as seawater gradually withdrew towards the southeast, its impact on the sedimentary environment significantly weakened, the sedimentary facies gradually evolved to the lagoon facies, tidal-flat facies, and swamp facies. Organic-rich lagoon shale occur in warm and humid environments, with shallow water bodies, weak evaporation, and low salinity. The input of terrestrial debris gradually increases compared to estuaries, and the overall sedimentation rate increases. The proportion of higher plant debris and clay minerals in terrestrial debris is high (Figure 1B). The bottom water of the lagoon facies is mainly in a weakly oxic environment, and due to limited nutrient supply, the paleo-productivity of the surface water is low. Organic matter mainly comes from terrestrial high plant debris, which has a slow decomposition rate during sedimentation and can effectively accumulate and preserve at a high sedimentation rate. Therefore, the types of organic matter in this environment are mainly II_2 and III (He et al., 2022).

Chemical weathering

In order to accurately characterize the chemical weathering intensity during the sedimentary period of Shanxi shale (Figure 6), widely used chemical weathering indicators were calculated (Deng et al., 2019). Due to the influence of indicator types and principles, there is no consistency in the trend of different weathering indicators. In addition, paleoclimate indicators do not match the commonly used trend of CIA changes. According to previous research, provenances, tectonic processes, transport efficiency, grain size, sedimentary cycles, hydrodynamic sorting, and diagenetic alteration all affect the chemical weathering index (Borges et al., 2009; von Eynatten et al., 2012; Garzanti and Resentini, 2016; Liu et al., 2022). Therefore, when linking chemical weathering with paleoclimate, the influence of the above factors must be excluded.

The average values of indicators such as CIA, CIW, and CIX reflect that the intensity of paleoweathering is highest in Unit 3 and lowest in Unit 1. However, the chemical strength within the same unit is also not stable, with the chemical strength gradually decreasing in Unit 1 and increasing in Unit 3. The A-CN-K triangle diagram proposed by Fedo et al. (1995) shows that most samples have undergone strong chemical weathering (CIA>80) (Figure 7A), possibly due to the continuous weathering of granodiorite parent rocks. Some sample points are biased towards point A, indicating strong kaolinization in the samples. In order to avoid hydrodynamic separation bias (Garzanti et al., 2013), the calculated α^{Al} values were compared and migration sequences of different elements were obtained (Figure 7B). The result shows $\alpha^{Al}_{Na} > \alpha^{Al}_{Ca} > \alpha^{Al}_{K} > \alpha^{Al}_{Ba} > \alpha^{Al}_{Rb} \geq \alpha^{Al}_{Sr} > \alpha^{Al}_{Mg}$. Principal component analysis was conducted on K_2O, Na_2O, CaO, Rb, Sr, Ba, and difficult to migrate Al_2O_3, SiO_2, as well as different α^{Al} values controlled by the source, which are sensitive to weathering intensity (Deng et al., 2019).

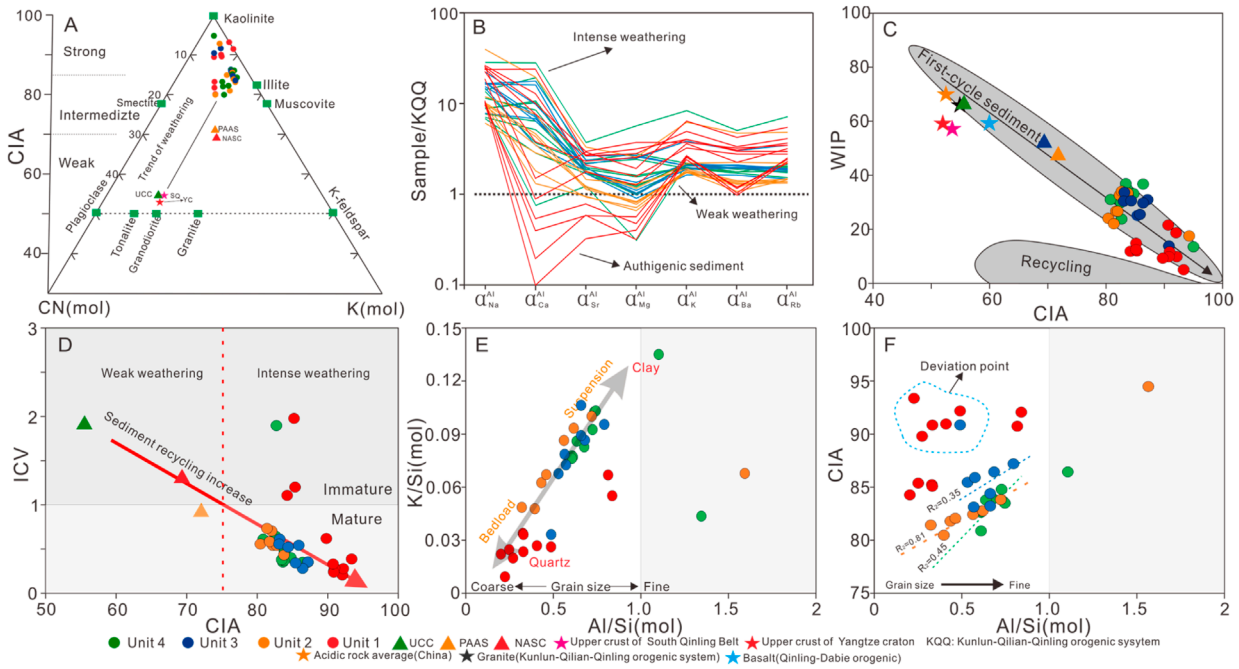

FIGURE 7
Plots of **(A)** A-CN-K ternary diagram with CIA values on the vertical axis. **(B)** Mobility of alkali/alkaline earth elements during chemical weathering. α^{Al}_{E} = [Al/E]sediment/[Al/E]source rock (Garzanti et al., 2013), E represent element of Na, Ca, Sr, Mg, K, Ba and Rb. **(C)** CIA-WIP cross-plot can assess the influence of recycling, quartz dilution affects WIP strongly but not CIA, the CIA/WIP plot readily reveals quartz enrichment in sediments. Study area mostly plot well below and near the field of first-cycle detritus (Garzanti et al., 2014). **(D)** CIA-ICV cross-plot, ICV decreases due to input of recycling of sedimentary material and CIA increasing due to intense weathering (Cox et al., 1995). **(E)** Hydraulic sorting effect on the Si–Al–K chemical composition of sediments (adapted from Lupker et al., 2013). **(F)** Grain size effect on CIA.

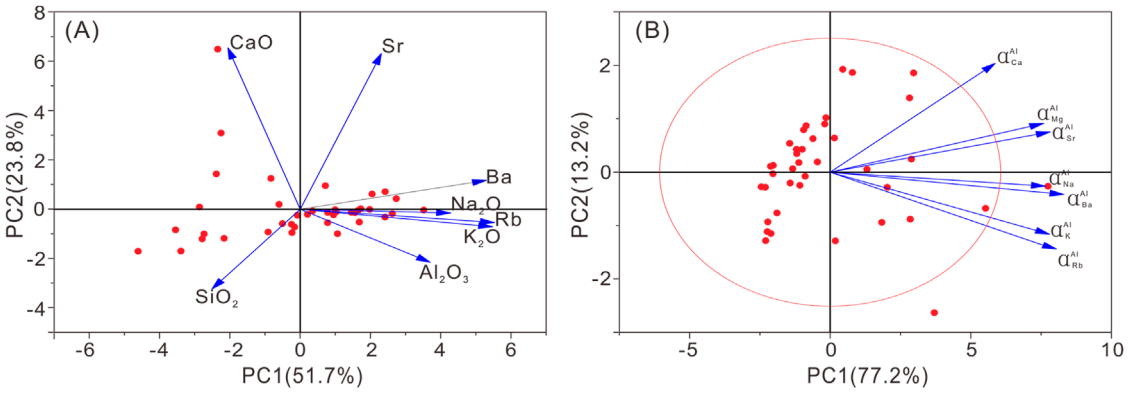

FIGURE 8
Biplots for the shale **(A)** to discriminate between strongly weathered sediments and less altered sediments in the Shanxi shale. **(B)** α^{Al} values (calculated with reference to the UCC standard for all samples) used to discriminate between dominantly provenance-controlled vs. weathering-controlled compositional variations.

Figure 8 indicates that the Shanxi shale cannot be distinguished by the aggregation of Al_2O_3, which may reflect a mixture of weathering intensity, recycling degree, and quartz dilution degree (Schneider et al., 2016; Deng et al., 2019). Different α^{Al} values are positively correlated with each other (Figure 8), indicating that the differences in sediment components are mainly controlled by weathering rather than provenance control (Deng et al., 2019).

In Figure 7C, the shale samples in Unit 1 estuarine facies closed to recycling zone, they may be affected by multiple-cyclic sedimentation, while other units are mostly formed by initial sedimentation (Garzanti et al., 2014). The index of compositional variability (ICV) of the samples in Figure 7D is generally less than 1, with a few samples are greater than 1, it indicate that the samples are compositionally mature and experienced intense weathering (CIA > 75) mostly. Therefore, they may primarily dominated by recycling effects and have a source of recycled sediment (Cox et al., 1995). The Th/Sc and Zr/Sc ratios in Figure 9E also indicate the recycling processes, as evidenced by an increase in zircon content

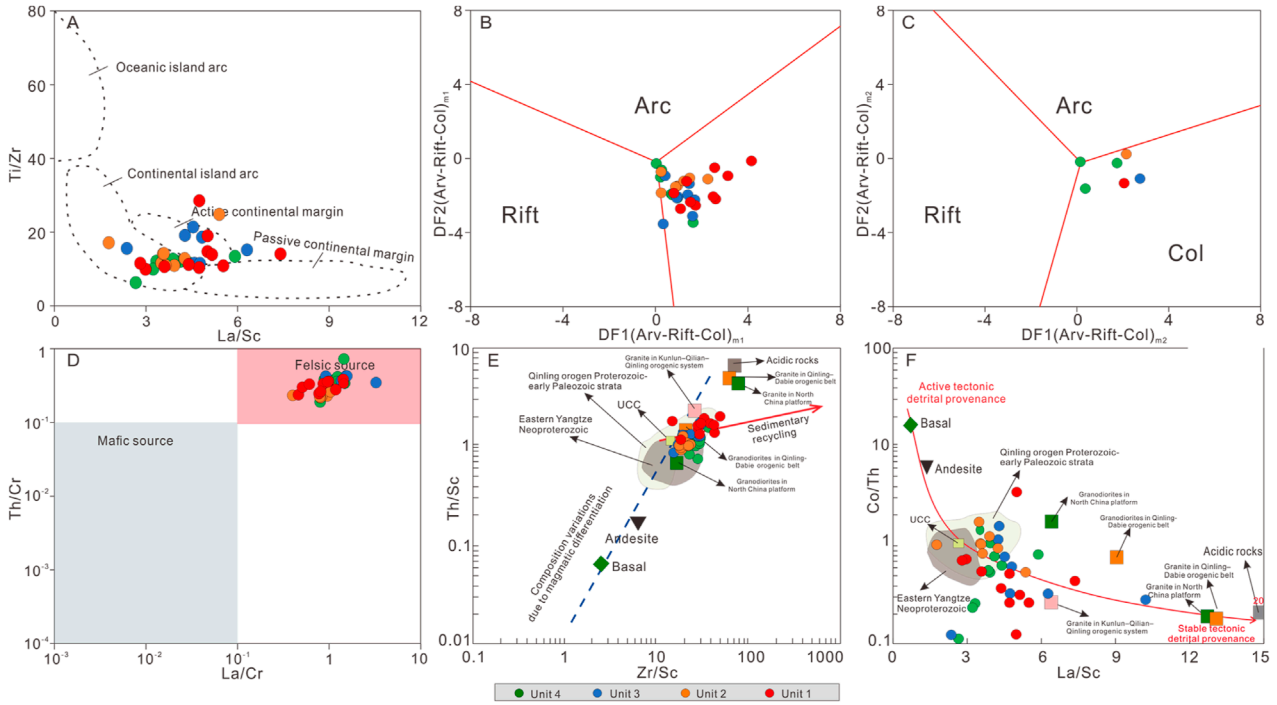

FIGURE 9
(A) Binary plot of La/Sc and Ti/Zr howing the paleotectonic setting for the studied samples (Bhatia and Crook, 1986). **(B, C)** Multidimensional diagram from Verma and Armstrong-Altrin (2009) for discrimination of high-silica (63% ≤ SiO2 ≥ 95%) and low-silica (35% ≤ SiO2 < 63%) tectonic settings, respectively. Plots of **(D)** Th/Cr-La/Cr (after Large et al., 2018) **(E)** Th/Sc–Zr/Sc diagram (after Mclennan et al., 1993) and **(F)** La/Sc–Co/Th diagram (after Lu et al., 2017) showing the provenanve for the Shanxi shale samples.

in Unit 1. Based on comprehensive analysis, it is believed that the environment of the Unit1 estuary exhibit high compositional maturity because of the recycling of marine sediments (Deng et al., 2019). Lupker et al. (2013) proposed that the Al/Si ratio can be used as a proxy for grain size to study the sorting effect of detrital sediments. There is a positive correlation between the Al/Si and K/Si ratios in Unit 2–4 (Al/Si < 1) except for two abnormal high values (Figure 7E), it indicating that the chemical weathering indicators of sediments are substantially affected by the sediment sorting effects during transportation and sedimentation processes in lagoon facies. However, in Unit 1, the correlation between the Al/Si and K/Si ratios is weak, it indicates that the esturaline facies shale is weakly affected by hydraulic sorting (Figure 7E). The CIA of Unit 2–4 has a certain correlation with Al/Si (excluding outliers > 1) (Figure 7F), which also indicates that chemical weathering indices seem to be influenced by grain size. In summary, the CIA of the Shanxi shale interval is influenced to varying degree by diagenetic alteration, sedimentary recycling, and hydrodynamic sorting, and is not directly a product of paleoclimate, as traditional concepts suggest.

Tectonic setting and provenance

The elemental geochemical data of sediments can also provide information on the tectonic background of sedimentary basins. The commonly used La/Sc vs. Ti/Zr intersection diagram indicates that the Shanxi shale samples were mainly deposited on the active continental margin and continental island arc areas (Figure 9A). In order to accurately determine the tectonic environment, this study used the high silicon and low silicon multidimensional maps reported in Verma and Armstrong-Altrin (2009) (Figures 9B, C). The high silicon and low silicon sample rocks in the study area are both located in the collision zone, indicating that the shale sedimentary period was an active continental margin, which is basically consistent with the peripheral tectonic environment of the Ordos Basin during this depositional period. The tectonic background corresponding to the evolution process of the Ordos Basin in the Early Permian is the subduction of the Paleo-Asian Ocean in the northern margin and the Mianlue Ocean Basin in the southern margin (Zhao et al., 2023).

The content of compatible elements Sc is relatively high in basic rocks, while incompatible elements Zr and Th are relatively high in acidic rocks. Therefore, La/Cr vs. Th/Cr, Zr/Sc vs. Th/SC, and La/SC vs. Co/Th can be used for parent rock type analysis (Mclennan et al., 1993; Large et al., 2018). In Figure 9D, the high ratio of La/Cr vs. Th/Cr indicates that the provenance region of Shanxi shale is acidic magmatic rock. The discrimination diagrams of Zr/Sc vs. Th/Sc and La/Sc vs. Co/Th (Figures 9E, F) both indicate that the Shanxi shale is mainly distributed within the range of granodiorite elements, and it can be determined that its parent rock is mainly granodiorite, which is consistent with the conclusion of Figure 7A. Furthermore, from a specific provenance, it is possible that it originated from the strata of the Qinling orogenic belt from the Proterozoic to Early Paleozoic (Lu et al., 2017).

Conclusion

(1) The transitional organic-rich shale of the Shanxi Formation can be divided into two types: the estuarine shale of Unit 1 and the lagoon shale of Unit 2–4. The average TOC of estuarine shale is significantly higher than that of lagoon shale, reaching 5.55%. The shale in estuaries is mainly deposited in suboxic-anoxic bottom water environments, with high surface productivity of seawater, which is conducive to the preservation of a large amount of organic matter. Lagoon shale is mainly composed of Type II_2 and III kerogen, with a weakly oxic bottom water environment. The paleoproductivity of the water surface is low, and the organic matter mainly comes from terrigenous high debris. Its fast sedimentation rate can effectively accumulate and preserve it.

(2) The calculation results of multiple chemical weathering indicators indicate that the chemical weathering indicators (such as CIA) of the Shanxi shale interval are controlled by sedimentary recycling, hydrodynamic sorting (including suspension separation and selective enrichment), and diagenetic alteration (kaolinization), with relatively small impacts from changes in the source area. The structural background and source analysis results indicate that the shale interval of the Shanxi Formation was mainly deposited on the active continental margin under collision background, with the main source being granodiorite from the Qinling orogenic belt.

Data availability statement

The raw data supporting the conclusions of this article will be made available by the authors, without undue reservation.

Author contributions

HZ: Conceptualization, Investigation, Methodology, Writing–original draft. YJ: Conceptualization, Investigation, Writing–review and editing. XL: Data curation, Formal Analysis, Funding acquisition, Writing–original draft. CJ: Investigation, Methodology, Validation, Visualization, Writing–review and editing. SL: Conceptualization, Data curation, Investigation, Methodology, Software, Supervision, Writing–review and editing. ZW: Conceptualization, Data curation, Investigation, Methodology, Writing–review and editing.

Funding

The author(s) declare that financial support was received for the research, authorship, and/or publication of this article. This study was funded by the National Natural Science Foundation of China (Grant No. 42272171), and the Science and Technology Cooperation Project of the CNPC-SWPU Innovation Alliance (Grant No. 2020CX030101).

Conflict of interest

Authors HZ, YJ, and ZW were employed by PetroChina Key Laboratory of Unconventional Oil and Gas Resources. Authors XL and SL were employed by PetroChina Coalbed Methane Company. Author CJ was employed by PetroChina Southwest Oil and Gas Field Company.

Publisher's note

References

Algeo, T. J., and Ingall, E. (2007). Sedimentary Corg:P ratios, paleocean ventilation, and Phanerozoic atmospheric pO2. *Palaeogeogr. Palaeoclimatol. Palaeoecol.* 256, 130–155. doi:10.1016/j.palaeo.2007.02.029

Algeo, T. J., and Liu, J. S. (2020). A re-assessment of elemental proxies for paleoredox analysis. *Chem. Geol.* 540, 119549. doi:10.1016/j.chemgeo.2020.119549

Bhatia, M. R., and Crook, K. A. W. (1986). Trace element characteristics of graywackes and tectonic setting discrimination of sedimentary basins. *Contrib. Mineral. Petrol.* 92 (2), 181–193. doi:10.1007/BF00375292

Böning, P., Brumsack, H. J., Böttcher, M. E., Schnetger, B., Kriete, C., Kallmeyer, J., et al. (2004). Geochemistry of Peruvian near-surface sediments. *Geochim. Cosmochim. Acta.* 68 (21), 4429–4451. doi:10.1016/j.gca.2004.04.027

Borges, J. B., Huh, Y., Moon, S., and Noh, H. (2009). Provenance and weathering control on river bed sediments of the eastern Tibetan Plateau and the Russian Far East. *Chem. Geol.* 254, 52–72. doi:10.1016/j.chemgeo.2008.06.002

Condie, K. C. (1993). Chemical composition and evolution of the upper continental crust: contrasting results from surface samples and shales. *Chem. Geol.* 104 (1), 1–37. doi:10.1016/0009-2541(93)90140-E

Cox, R., Lowe, D. R., and Cullers, R. L. (1995). The influence of sediment recycling and basement composition on evolution of mudrock chemistry in the southwestern United States. *Geochim. Cosmochim. Acta.* 59 (14), 2919–2940. doi:10.1016/0016-7037(95)00185-9

Deng, T., Li, Y., Wang, Z., Yu, Q., Dong, S., Yan, L., et al. (2019). Geochemical characteristics and organic matter enrichment mechanism of black shale in the Upper Triassic Xujiahe Formation in the Sichuan basin: implications for paleoweathering, provenance and tectonic setting. *Mar. Pet. Geol.* 109, 698–716. doi:10.1016/j.marpetgeo.2019.06.057

Fedo, C. M., Nesbitt, H. W., and Young, G. M. (1995). Unravelling the effects of potassium metasomatism in sedimentary rocks and paleosols, with implications for paleoweathering conditions and provenance. *Geology* 23 (10), 921–924. doi:10.1130/0091-7613(1995)023<0921:UTEOPM>2.3.CO;2

Gaillardet, J., Dupré, B., and Allègre, C. J. (1999). Geochemistry of large river suspended sediments: silicate weathering or recycling tracer? *Geochim. Cosmochim. Acta.* 63, 4037–4051. doi:10.1016/S0016-7037(99)00307-5

Gallagher, T. M., and Sheldon, N. D. (2013). A new paleothermometer for forest paleosols and its implications for Cenozoic climate. *Geology* 41 (6), 647–650. doi:10.1130/G34074.1

Garzanti, E., Padoan, M., Andò, S., Resentini, A., Vezzoli, G., and Lustrino, M. (2013). Weathering and relative durability of detrital minerals in equatorial climate: sand petrology and geochemistry in the east african rift. *J. Geol.* 121 (6), 547–580. doi:10.1086/673259

Garzanti, E., Padoan, M., Setti, M., López-Galindo, A., and Villa, I. M. (2014). Provenance versus weathering control on the composition of tropical river mud (southern Africa). *Chem. Geol.* 366, 61–74. doi:10.1016/j.chemgeo.2013.12.016

Garzanti, E., and Resentini, A. (2016). Provenance control on chemical indices of weathering (Taiwan river sands). *Sediment. Geol.* 336, 81–95. doi:10.1016/j.sedgeo.2015.06.013

Gu, Y. F., Li, X. T., Qi, L., Li, S. X., Jiang, Y. Q., Fu, Y. H., et al. (2022). Sedimentology and geochemistry of the lower permian Shanxi Formation Shan 2^3 submember transitional shale, eastern Ordos Basin, north China. *Front. Earth Sci.* 10, 859845. doi:10.3389/feart.2022.859845

Harnois, L. (1988). The CIW index: a new chemical index of weathering. *Sediment. Geol.* 55, 319–322. doi:10.1016/0037-0738(88)90137-6

He, Q. B., Chen, S. J., Li, S. X., Guo, B. Z., Lu, J. G., Li, Y., et al. (2022). Organic geochemical characteristics and hydrocarbon generation mechanism of marine-continental transitional organic-rich shale: a case study from the Shanxi formation in the eastern margin of the Ordos Basin. *J. Pet. Sci. Eng.* 219, 111116. doi:10.1016/j.petrol.2022.111116

Jiang, Y., Wen, S., Cai, G., Li, s., Xiong, X., Li, X., et al. (2023). Lithologic assemblage characteristics and shale gas exploration potential of transitional shale in the Ordos Basin. *Nat. Gas. Ind.* 43 (4), 62–75. doi:10.3787/j.issn.1000-0976.2023.04.007

Jiao, F., Wen, S., Liu, X., Xiong, X., Li, S., Gu, Y., et al. (2023). Research progress in exploration theory and technology of transitional shale gas in the Ordos Basin. *Nat. Gas. Ind.* 43 (4), 11–23. doi:10.3787/j.issn.1000-0976.2023.04.002

Jones, B., and Manning, D. A. C. (1994). Comparison of geochemical indices used for the interpretation of palaeoredox conditions in ancient mudstones. *Chem. Geol.* 111 (1), 111–129. doi:10.1016/0009-2541(94)90085-X

Kuang, L. C., Dong, D. Z., He, W. Y., Wen, S. M., Sun, S. S., Li, S. X., et al. (2020). Geological characteristics and development potential of transitional shale gas in the east margin of the Ordos Basin, NW China. *Pet. Explor. Dev.* 47 (3), 471–482. doi:10.1016/S1876-3804(20)60066-0

Large, R. R., Mukherjee, I., Zhukova, I., Corkrey, R., Stepanov, A., and Danyushevsky, L. V. (2018). Role of upper-most crustal composition in the evolution of the Precambrian ocean–atmosphere system. *Earth Planet. Sci. Lett.* 487 (1), 44–53. doi:10.1016/j.epsl.2018.01.019

Lei, W. Z., Chen, D. X., Liu, Z. Y., and Cheng, M. (2023). Paleoenvironment-driven organic matter accumulation in lacustrine shale mixed with shell bioclasts: a case study from the Jurassic Da'anzhai member, Sichuan Basin (China). *J. Pet. Sci. Eng.* 220, 111178. doi:10.1016/j.petrol.2022.111178

Li, Q., Wu, S. H., Xia, D. L., You, X. L., Zhang, H. M., and Lu, H. (2020). Major and trace element geochemistry of the lacustrine organic-rich shales from the Upper Triassic Chang 7 Member in the southwestern Ordos Basin, China: implications for paleoenvironment and organic matter accumulation. *Mar. Pet. Geol.* 111, 852–867. doi:10.1016/j.marpetgeo.2019.09.003

Liu, R. P., Hu, G., Cao, J., Yang, R. F., Liao, Z. W., Hu, C. W., et al. (2022). Enhanced hydrological cycling and continental weathering during the Jenkyns Event in a lake system in the Sichuan Basin, China. *Glob. Planet. Change* 216, 103915. doi:10.1016/j.gloplacha.2022.103915

Liu, W., Zhao, Q., Qiu, Z., Zhao, P., Li, S., Dong, D., et al. (2023). Research status and prospect of accumulation conditions of transitional facies shale gas in the easten margin of Ordos Basin. *Nat. Gas. Geosci.* 34 (5), 868–887. doi:10.11764/j.issn.1672-1926.2022.11.001

Lodders, K., and Fegley, Jr. B. (1998). *The planetary scientist's companion*. Oxford University Press.

Lu, Y., Zhao, Z., and Zheng, Y. (2017). Geochemical constraints on the nature of magma sources for Triassic granitoids from South Qinling in central China. *Lithos* 284-285 (2017), 30–49. doi:10.1016/j.lithos.2017.03.028

Lupker, M., France-Lanord, C., Galy, V., Lavé, J., and Kudrass, H. (2013). Increasing chemical weathering in the himalayan system since the last glacial maximum. *Earth Planet. Sci. Lett.* 365 (1), 243–252. doi:10.1016/j.epsl.2013.01.038

McLennan, S. M., Hemming, S., McDaniel, D. K., and Hanson, G. N. (1993). Geochemical approaches to sedimentation, provenance, and tectonics. *Geol. Soc. Am. Spec. Pap.* 284, 21–40. doi:10.1130/SPE284-p21

Nesbitt, H. W., and Young, G. M. (1982). Early Proterozoic climates and plate motions inferred from major element chemistry of lutites. *Nature* 299 (5885), 715–717. doi:10.1038/299715a0

Pan, X., Wang, Z. L., Li, Q. Y., Gao, J., Zhu, L. W., and Liu, W. H. (2020). Sedimentary environments and mechanism of organic matter enrichment of dark shales with low TOC in the Mesoproterozoic Cuizhuang Formation of the Ordos Basin: evidence from petrology, organic geochemistry, and major and trace elements. *Mar. Pet. Geol.* 122, 104695. doi:10.1016/j.marpetgeo.2020.104695

Parker, A. (1970). An index of weathering for silicate rocks. *Geol. Mag.* 107 (6), 501–504. doi:10.1017/S0016756800058581

Qiu, Z., and He, J. L. (2022). Depositional environment changes and organic matter accumulation of Pliensbachian-Toarcian lacustrine shales in the Sichuan basin, SW China. *J. Asian Earth Sci.* 232, 105035. doi:10.1016/j.jseaes.2021.105035

Rasmussen, C., Brantley, S., Richter, D. B., Blum, A., Dixon, J., and White, A. F. (2011). Strong climate and tectonic control on plagioclase weathering in granitic terrain. *Earth Planet. Sci. Lett.* 301, 521–530. doi:10.1016/j.epsl.2010.11.037

Rimmer, S. M. (2004). Geochemical paleoredox indicators in devonian-mississippian black shales, central appalachian basin (USA). *Chem. Geol.* 206 (3), 373–391. doi:10.1016/j.chemgeo.2003.12.029

Schneider, S., Hornung, J., Hinderer, M., and Garzanti, E. (2016). Petrography and geochemistry of modern river sediments in an equatorial environment (Rwenzori Mountains and Albertine rift, Uganda)—implications for weathering and provenance. *Sediment. Geol.* 336, 106–119. doi:10.1016/j.sedgeo.2016.02.006

Schoepfer, S. D., Shen, J., Wei, H. Y., Tyson, R. V., Ingall, E., and Algeo, T. J. (2015). Total organic carbon, organic phosphorus, and biogenic barium fluxes as proxies for paleomarine productivity. *Earth Sci. Rev.* 149, 23–52. doi:10.1016/j.earscirev.2014.08.017

Sun, L., Zhang, J. L., Li, Y., Yan, X., and Zhang, X. C. (2022). Paleosalinity and lake level fluctuations of the 3rd member of paleogene shahejie formation, chezhen sag, bohai bay basin. *Front. Earth Sci.* 16 (4), 949–962. doi:10.1007/s11707-022-0979-0

Tan, J., Jiang, Y., Li, X., Ji, C., Gu, Y., and Wang, Z. (2023). Paleoenvironment of marine-continental transitional shales in the lower Permian Shanxi formation, southeastern Ordos Basin, China. *Energy Geosci.* 5 (2024), 100261. doi:10.1016/j.engeos.2023.100261

Tribovillard, N., and Algeo, T. J. (2009). Environmental analysis of paleoceanographic systems based onmolybdenum-uranium covariation. *Chem. Geol.* 268 (3), 211–225. doi:10.1016/j.chemgeo.2009.09.001

Tribovillard, N., Algeo, T. J., Lyons, T., and Riboulleau, A. (2007). Trace metals as paleoredox and paleoproductivity proxies: an update. *Chem. Geol.* 232 (1), 12–32. doi:10.1016/j.chemgeo.2006.02.012

Tyson, R. V. (2001). Sedimentation rate, dilution, preservation and total organic carbon: some results of a modelling study. *Org. Geochem.* 32 (2), 333–339. doi:10.1016/S0146-6380(00)00161-3

Verma, S. P., and Armstrong-Altrin, J. S. (2009). New multi-dimensional diagrams for tectonic discrimination of siliciclastic sediments and their application to Precambrian basins. *Chem. Geol.* 355, 117–133. doi:10.1016/j.chemgeo.2013.07.014

von Eynatten, H., Tolosana-Delgado, R., and Karius, V. (2012). Sediment generation in modern glacial settings: grain-size and source-rock control on sediment composition. *Sediment. Geol.* 280, 80–92. doi:10.1016/j.sedgeo.2012.03.008

Wang, X., Zhou, L., Wu, Y., Zhang, X., Li, S., Li, Y., et al. (2023). Restoration of palaeogeomorphology and its petroleum-geological significance: transitional-facies deposition during the early Permian in the southeastern Ordos Basin, North China. *J. Petrol. Sci. Eng.* 221 (2023), 111310. doi:10.1016/j.petrol.2022.111310

Wedepohl, K. H. (1995). The composition of the continental crust. *Geochim. Cosmochim. Acta.* 59, 1217–1232. doi:10.1016/0016-7037(95)00038-2

Wei, W., and Algeo, T. J. (2019). Elemental proxies for paleosalinity analysis of ancient shales and mudrocks. *Geochim. Cosmochim. Acta.* 287, 341–366. doi:10.1016/j.gca.2019.06.034

Wei, W., Algeo, T. J., Lu, Y. B., Lu, Y. C., Liu, H. M., Zhang, S. P., et al. (2018). Identifying marine incursions into the Paleogene Bohai Bay Basin lake system in northeastern China. *Int. J. Coal Geol.* 200, 1–17. doi:10.1016/j.coal.2018.10.001

Wu, J., Wang, H. Y., Shi, Z. S., Wang, Q., Zhao, Q., Dong, D. Z., et al. (2021). Favorable lithofacies types and genesis of marine-continental transitional black shale: a case study of Permian Shanxi Formation in the eastern margin of Ordos Basin, NW China. *Pet. Explor. Dev.* 48 (6), 1315–1328. doi:10.1016/S1876-3804(21)60289-6

Wu, Z. Y., Pu, X. G., Tao, X. W., Shi, Z. N., and Sun, Y. Z. (2021). Paleoenvironmental modes and organic matter enrichment mechanisms of lacustrine shale in the paleogene shahejie formation, qikou sag, bohai bay basin. *Energy Rep.* 7, 9046–9068. doi:10.1016/j.egyr.2021.11.228

Xu, F. Y., Wang, C. W., Xiong, X. Y., Xu, B. R., Wang, H. N., Zhao, X., et al. (2023). Evolution law of deep coalbed methane reservoir formation and exploration and development practice in the eastern margin of Ordos Basin (In Chinese with English abstract). *Acta Pet. Sin.* 44 (11), 1764–1780. doi:10.7623/syxb202311002

Xu, S. C., Hu, H. B., Zhang, P., Wang, Q. C., Kang, J., and Miao, Q. (2020). Major and trace elements in mid-Eocene lacustrine oil shales of the Fushun Basin, NE China: concentration features and paleolimnological implications. *Mar. Pet. Geol.* 121, 104610. doi:10.1016/j.marpetgeo.2020.104610

Yang, S. L., Ding, F., and Ding, Z. L. (2006). Pleistocene chemical weathering history of Asian arid and semi-arid regions recorded in loess deposits of China and Tajikistan. *Geochim. Cosmochim. Acta.* 70 (7), 1695–1709. doi:10.1016/j.gca.2005.12.012

Zhang, L. F., Dong, D. Z., Qiu, Z., Wu, C. J., Zhang, Q., Wang, Y. M., et al. (2021). Sedimentology and geochemistry of Carboniferous-Permian marine-continental transitional shales in the eastern Ordos Basin, North China. *Palaeogeogra. Palaeoclimatol. Palaeoecol.* 571, 110389. doi:10.1016/j.palaeo.2021.110389

Zhang, Q., Qiu, Z., Zhang, L. F., Wang, Y. M., Xiao, Y. F., Liu, D., et al. (2022). Characteristics and controlling factors of transitional shale gas reservoirs: an example from Permian Shanxi Formation, Daning-Jixian block, Ordos Basin, China. *Nat. Gas. Geosci.* 7 (3), 147–157. doi:10.1016/j.jnggs.2022.06.004

Zhao, B. S., Li, R. X., Qin, X. L., Wang, N., Zhou, W., Khaled, A., et al. (2021). Geochemical characteristics and mechanism of organic matter accumulation of marine-continental transitional shale of the lower permian Shanxi Formation, southeastern Ordos Basin, north China. *J. Petrol. Sci. Eng.* 205, 108815. doi:10.1016/j.petrol.2021.108815

Zhao, J. H., Jin, Z. K., Jin, Z. J., Wen, X., and Geng, Y. K. (2017). Origin of authigenic quartz in organic-rich shales of the wufeng and longmaxi formations in the sichuan basin, south China: implications for pore evolution. *J. Nat. Gas. Sci. Eng.* 38, 21–38. doi:10.1016/j.jngse.2016.11.037

Zhao, Y., Gong, W., Hu, J., Chen, H., Wang, D., and Yang, Y. (2023). The uplift of Fuping Complex and its implications for the late Paleoproterozoic evolution of the North China Craton. *Precambrian Res.* 394 (2023), 107061. doi:10.1016/j.precamres.2023.107061

Zou, C. N., Pan, S. Q., Jing, Z. H., Gao, J. L., Yang, Z., Wu, S. T., et al. (2020). Shale oil and gas revolution and its impact (In Chinese with English abstract). *Acta Pet. Sin.* 41 (1), 1–12. doi:10.7623/syxb202001001

Zou, C. N., Qiu, Z., Zhang, J. Q., Li, Z. Y., Wei, H. Y., Liu, B., et al. (2022). Unconventional petroleum sedimentology: a key to understanding unconventional hydrocarbon accumulation. *Engineering* 18, 62–78. doi:10.1016/j.eng.2022.06.016

Zou, C. N., Zhu, R. K., Chen, Z. Q., Ogg, J. G., Wu, S. T., Dong, D. Z., et al. (2019). Organic-matter-rich shales of China. *Earth Sci. Rev.* 189, 51–78. doi:10.1016/j.earscirev.2018.12.002